Modeling and Control of a Hovering Mini Tail-Sitter

Pierre-Richard Bilodeau and Franklin Wong
AEREX Avionics Inc., Breakeyville, Quebec, QC, Canada;
Defence R&D Canada Valcartier, Quebec, QC, Canada

[Received date; Accepted date] – to be inserted later

Abstract
A systematic approach to characterize and control the attitude of a hovering tail-sitter mini-aerial vehicle (TS-MAV) is developed. A model of the TS-MAV dynamics is formulated by decoupling and linearizing a nonlinear model based on quaternions. Identification of the model parameters was carried out using a prediction error method and flight test data. Two control structures were synthesized to examine the benefits of using an anti-windup proportional-integral regulator in the inner control loop rather than in the outer control loop. It was found that a regulator in the inner loop reduced overshoot and eliminated an unstable pole. Flight tests with a TS-MAV test bed showed that a nine percent overshoot was reduced to zero thereby demonstrating the enhanced responsiveness of the vehicle using this control strategy.

1. INTRODUCTION

The Canadian Forces has been examining how mini air vehicles (MAVs) may be employed by soldiers in future operations to support the capabilities required for the Army of Tomorrow [1]. As a result, the Canadian Forces Integrated Soldier System Project [2] has an objective of providing the soldier with an integrated suite of equipment that includes backpackable aerial and ground sensors, weapons, battle management devices, operational clothing and personal protection. This study was motivated by the fact that camera-carrying MAVs were identified as an asset that the future soldier will carry to improve his situational awareness in urban environments.

There are three essential criteria for any soldier-carried airborne sensor: 1) it must be able to fly at very low forward speed, 2) it must be structurally robust, and 3) it must be able to fly by itself. To address the first two points, several types of MAVs have been developed in the past. Fixed-wing designs are structurally robust but they cannot fly at very slow forward speeds in standard attitudes. Rotorcraft designs can fly slowly except their mechanical control system is not structurally robust in comparison to a fixed-wing design. An alternative to these two types of platforms is a platform that is capable of hybrid mode flight. For example, if a high performance lightweight fixed-wing MAV can be commanded to execute fast level flight or to execute a maneuver known as 'prop hanging' or 'hovering' for slow forward flight, the characteristics of structural robustness and slow flight may be obtained with a fixed-wing design. Manually piloting a fixed-wing MAV to hover for an extended length of time takes great concentration and skill. If the hovering maneuver can be automated, then it is possible to create a robust, slow flying airborne sensor that a soldier can use with little effort.

In previous studies by Bilodeau [3] and Bilodeau et al. [4], a control architecture was developed for a fixed-wing MAV with an onboard wireless inertial measurement unit (IMU) and an offboard controller. A state machine architecture based on [3] and [4] was developed by Myrand-Lapierre et al. [5] and Myrand-Lapierre [6] to automate the transitions between hover and level flight of a fixed-wing MAV. Bumpless control architecture was implemented to attenuate sudden command changes introduced by states changes. Satisfactory flight performance results were obtained. However, it was observed that aileron positioning created a challenge for the elevator control design. When the ailerons were activated to counter the motor torque in hover, the ailerons would shadow the elevator and cause a change in the available elevator control authority in comparison to the control authority present when the ailerons were in their neutral position during level flight

and transitioning.

A variation of the classic fixed-wing configuration is a tail-sitter configuration like the Convair XFY-1 Pogo [7]. This vehicle possesses a rudder, but has elevons instead of ailerons and an elevator. With this kind of design, the structure of the air stream across the empennage control surfaces remains the same whether the platform is in hover or level flight because there is no shadowing effect on the elevator. The elevator control design for this type of airframe should, therefore, be much simpler.

In [8], Stone presented a control architecture for a tail-sitter powered by twin gasoline engines. It was capable of maneuvering in both hovering and level flight modes. For hovering mode, longitudinal and lateral control was achieved with linear quadratic regulators (LQR) while the roll and altitude control was achieved with proportional-integral-derivative (PID) regulators. Level flight controllers were designed with classical SISO root locus techniques. A model of the tail-sitter dynamics was obtained using parameter identification techniques. Airframe attitude was calculated with two Euler angle representations to ensure that no mathematical singularities occurred between level flight and hovering modes. A smaller airframe, which is more similar to the one used in this paper, was controlled by Knobel et al. [9], Knobel [10] and Osborne [11] using two different control strategies. The performance of gain-scheduled PIDs, which were a function of the main air stream speed, was compared to the performance of adaptive controllers. Quaternions [12] were used to ensure uniformity in the control architecture and to avoid singularities as the airframe transitioned between level flight and hovering attitudes. The results showed that adaptive controllers did not have a great advantage in performance over well-tuned PIDs. It is worth noting that their PIDs were implemented with a cascaded approach where the derivative term was replaced with a rate gyro inner loop. In similar control applications involving MAVs, many authors (Green [13], Frank et al. [14], DeBlauwe et al. [15]) retained LQR tuning techniques and PIDs to stabilize their vehicles. However, none of them proposed a cascaded control structure with a proportional-integral (PI) controller in the inner loop because this configuration removes 90 degrees of phase margin thus diminishing available margin for the outer loop. Placing a PI controller in the inner loop is less intuitive but it offers some advantages as will be demonstrated in this paper.

The objectives of this paper are to illustrate a systematic approach for modeling and controlling a hovering tail-sitter mini-aerial vehicle (TS-MAV). A model of the TS-MAV is formulated and used to compare two cascaded controller configurations. The identification of the longitudinal model parameters is presented and is followed by analysis of the controllers. Flight test results are shown to demonstrate the effectiveness of the proposed control architectures.

2. MODELING

A modeling approach, similar to the one proposed by Stone [8], is employed to derive model equations in terms of quaternions for a TS-MAV for a hovering orientation. Only the model structure for the longitudinal mode is presented for the sake of brevity.

1.1 Non-Linear Model

The quaternion-based nonlinear model [16] is given by

$$\dot{\mathbf{v}} = \mathbf{v} \times \boldsymbol{\Omega} + \mathbf{q}^* p(\mathbf{g}) + \frac{\mathbf{F}}{m} \tag{1}$$

$$\dot{\boldsymbol{\Omega}} = \mathbf{J}^{-1}\left(\mathbf{M} - \boldsymbol{\Omega} \times \mathbf{J} \times \boldsymbol{\Omega}\right) \tag{2}$$

$$\dot{\mathbf{q}} = \frac{1}{2}\mathbf{q} p(\boldsymbol{\Omega}) \tag{3}$$

where $\mathbf{v}$, $\boldsymbol{\Omega}$ and $\mathbf{q}$ express the displacement speeds (u, v, w), angular rates (ω_x, ω_y, ω_z) and quaternion (q_w, q_x, q_y, q_z), respectively. $\mathbf{J}$ is the inertia matrix where only the diagonal terms (J_x, J_y, J_z) are retained while $\mathbf{g}$ is the gravitational acceleration vector expressed in the inertial frame. The operator $p(\ )$ converts a three dimensional vector into a pure quaternion where the scalar component equals zero. $\mathbf{F}$ and $\mathbf{M}$ are the external forces (F_x, F_y, F_z) and moments (L, M, N)

applied to the center of mass. m expresses the mass of the vehicle. It is worth noting that all variables except $\mathbf{g}$ are expressed in the body frame. Figure 1 illustrates the body frame and variables described above.

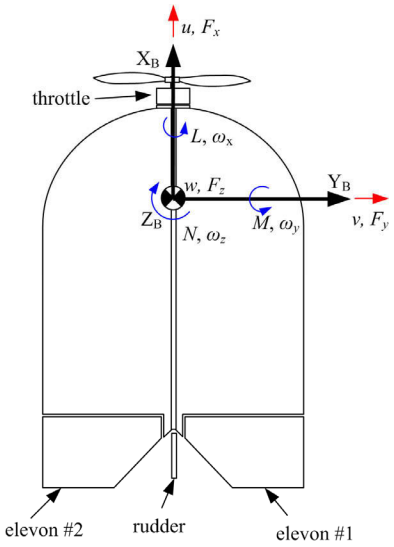

Figure 1. Body frame definition

1.2 Error Quaternion

The error quaternion $\mathbf{q}^e$ is the difference between the desired quaternion $\mathbf{q}^d$ and the measured quaternion $\mathbf{q}^m$. $\mathbf{q}^e$ is given by

$$\mathbf{q}^e = \left(\mathbf{q}^m\right)^{-1}\mathbf{q}^d \tag{4}$$

The quantity $\mathbf{q}^e$ is used for control only. For modeling, $\mathbf{q}^m$ is isolated and assumed equal to the current attitude $\mathbf{q}$ such that

$$\mathbf{q} = \mathbf{q}^m = \mathbf{q}^d\left(\mathbf{q}^e\right)^{-1} \tag{5}$$

In hovering mode, $\mathbf{q}^d$ is assumed equal to the vertical quaternion such that

$$\mathbf{q}^d = \mathbf{q}^v = [0.7071,0,0.7071,0]^T \tag{6}$$

Substituting eqn. (6) in eqn. (5) gives

$$\begin{bmatrix} q_w \\ q_x \\ q_y \\ q_z \end{bmatrix} = \begin{bmatrix} 0.7071q_w^e + 0.7071q_y^e \\ -0.7071q_x^e - 0.7071q_z^e \\ 0.7071q_w^e - 0.7071q_y^e \\ 0.7071q_x^e - 0.7071q_z^e \end{bmatrix} \tag{7}$$

1.3 Decoupling and Simplification of the Model Equations in Hover Orientation

Assuming that the vehicle is operating in hovering mode with no vertical speed (u=0) and using a body axis system, the relevant longitudinal state variables are w, ω_y and q_y^e. Thus, the relevant nonlinear eqns. (1) - (3) become

$$\dot{w} = \omega_y u - \omega_x v + \left(2q_w^e q_y^e - 2q_x^e q_z^e\right)g + F_z/m \quad (8)$$

$$\dot{\omega}_y = \left((J_z - J_x)\omega_x\omega_z + M\right)/J_y \quad (9)$$

$$\dot{q}_y^e = -0.5\left(\omega_y q_w^e - \omega_z q_x^e + \omega_x q_z^e\right) \quad (10)$$

These equations can be simplified by assuming that all state variables are equal to small perturbations around a null operation point and by assuming that in closed loop $\mathbf{q}^e \to [1.0, 0.0, 0.0, 0.0]^T$. Therefore, when multiplying two vector components of q_i^e, where i = x, y, z, the result is small and can be neglected. However, if q_w^e is multiplied by a vector component, the result is approximately equal to the vector component itself (e.g. $q_w^e q_y^e \approx q_y^e$). This simplification can also be applied to other states multiplied together. By applying these simplifications, the longitudinal model becomes

$$\dot{w} = 2q_y^e g + F_z/m \quad (11)$$

$$\dot{\omega}_y = M/J_y \quad (12)$$

$$\dot{q}_y^e = -0.5\omega_y \quad (13)$$

1.4 Linearization

Linearization is carried out with a first-order Taylor series expansion. The selected variables of interest are the three longitudinal state variables w, ω_y and q_y^e and the elevon input variables, δ_{elv1} and δ_{elv2}, which interact with these states

$$\Delta\dot{w} = \frac{1}{m}\frac{\partial F_z}{\partial w}\Delta w + \frac{1}{m}\frac{\partial F_z}{\partial \omega_y}\Delta\omega_y + 2g\Delta q_y^e + \frac{1}{m}\frac{\partial F_z}{\partial \delta_{elv1}}\Delta\delta_{elv1} + \frac{1}{m}\frac{\partial F_z}{\partial \delta_{elv2}}\Delta\delta_{elv2} \quad (14)$$

$$\Delta\dot{w} \cong \overline{F}_{zw}\Delta w + \overline{F}_{\omega_y}\Delta\omega_y + 2g\Delta q_y^e + \overline{F}_{z\delta_{elv1}}\Delta\delta_{elv1} + \overline{F}_{z\delta_{elv2}}\Delta\delta_{elv2} \quad (15)$$

$$\Delta\dot{\omega}_y = \frac{1}{J_y}\frac{\partial M}{\partial w}\Delta w + \frac{1}{J_y}\frac{\partial M}{\partial \omega_y}\Delta\omega_y + \frac{1}{J_y}\frac{\partial M}{\partial \delta_{elv1}}\Delta\delta_{elv1} + \frac{1}{J_y}\frac{\partial M}{\partial \delta_{elv2}}\Delta\delta_{elv2} \quad (16)$$

$$\Delta\dot{\omega}_y \cong \overline{M}_w\Delta w + \overline{M}_{\omega_y}\Delta\omega_y + \overline{M}_{\delta_{elv1}}\Delta\delta_{elv1} + \overline{M}_{\delta_{elv2}}\Delta\delta_{elv2} \quad (17)$$

$$\Delta\dot{q}_y^e = -0.5\Delta\omega_y \quad (18)$$

By dropping the Δ notation, the longitudinal dynamic can be expressed by the following state space (SS) model [17]

$$\begin{bmatrix} \dot{w} \\ \dot{\omega}_y \\ \dot{q}_y^e \end{bmatrix} = \begin{bmatrix} \overline{F}_{zw} & \overline{F}_{\omega_y} & 2g \\ \overline{M}_w & \overline{M}_{\omega_y} & 0 \\ 0 & -0.5 & 0 \end{bmatrix} \begin{bmatrix} w \\ \omega_y \\ q_y^e \end{bmatrix} + \begin{bmatrix} \overline{F}_{z\delta_{elv1}} & \overline{F}_{z\delta_{elv2}} \\ \overline{M}_{\delta_{elv1}} & \overline{M}_{\delta_{elv2}} \\ 0 & 0 \end{bmatrix} \begin{bmatrix} \delta_{elv1} \\ \delta_{elv2} \end{bmatrix} \quad (19)$$

3. DESCRIPTION OF THE TAIL-SITTER TESTBED

As illustrated in Figure 2, the TS-MAV testbed is a custom tail-sitter which has an all-up weight of 390 grams without batteries. The propulsion system consists of a Hyperion HP-Z2209-32 brushless motor coupled to a 25 A electronic speed controller and a 9 x 4.5 in. propeller. A 75 grams, 11.1 V, 800 mAh Li-Po battery provides power.

A programmable onboard autopilot, with a refresh rate of 50 Hz, is used to estimate and control the attitude. The actual refresh rate in the autopilot is sufficient to sample the control surface movements which were in the range of 5-8 Hz. The attitude estimator [18] uses data from the autopilot's three accelerometers and three rate gyros. The aerodynamic surfaces (two elevons and

one rudder) as well as the throttle are directly controlled by the autopilot. A wireless ground control station is used to transmit operator setpoints, read from a handheld controller, to the autopilot.

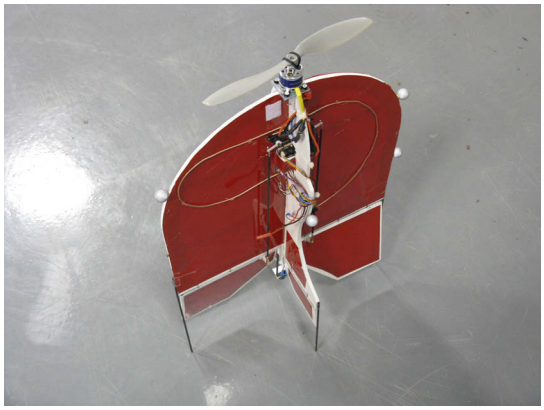

Figure 2. TS-MAV testbed

4. IDENTIFICATION

The identification of the unknown model parameters in eq. (19) was carried out with the prediction error method (PEM) [19]. For the identification of the longitudinal model, the SS structure takes the following form

$$\dot{\mathbf{x}}(t) = \mathbf{A}\mathbf{x}(t) + \mathbf{B}\mathbf{u}(t) + \mathbf{K}\mathbf{e}(t) \tag{20}$$

$$\mathbf{y}(t) = \mathbf{C}\mathbf{x}(t) + \mathbf{D}\mathbf{u}(t) + \mathbf{e}(t) \tag{21}$$

where $\mathbf{K}$ is a disturbance matrix and $\mathbf{e}(t)$ is a Gaussian white noise vector. The matrix $\mathbf{A}$ and $\mathbf{B}$ contain the unknown parameters from eq. (19) to estimate. The matrix $\mathbf{C}$ was defined as follows

$$\mathbf{C} = \begin{bmatrix} 1 & 0 & 0 \\ 0 & 1 & 0 \\ 0 & 0 & 0 \end{bmatrix} \tag{22}$$

Therefore, only w and ω_y were used for identification. $\mathbf{x}$ specifies the observed outputs which were used for identification. In this case, w and ω_y were selected and measured by a vision system and a rate-gyro, respectively. $\mathbf{D}$ specifies if there is a direct transmission between inputs and outputs. For most physical processes, $\mathbf{D}$ is equal to zero, which is the case here. With this identification structure and the PEM, the identified longitudinal model, with parameter standard deviations presented in parentheses, is

$$\begin{bmatrix} \dot{w} \\ \dot{\omega}_y \\ \dot{q}_y^e \end{bmatrix} = \begin{bmatrix} -15.43(\pm 5.5) & -24.63(\pm 15) & 19.62 \\ -2.00(\pm 1.3) & -10.96(\pm 3.5) & 0 \\ 0 & -0.5 & 0 \end{bmatrix} \begin{bmatrix} w \\ \omega_y \\ q_y^e \end{bmatrix} + \begin{bmatrix} -72.654(\pm 6.7) & 72.654(\pm 5.5) \\ 25.30(\pm 2) & -25.30(\pm 5.5) \\ 0 & 0 \end{bmatrix} \begin{bmatrix} \delta_{elv1} \\ \delta_{elv2} \end{bmatrix} + \begin{bmatrix} 15.92(\pm 1.8) & 0 \\ 0 & 23.74(\pm 1.6) \\ 0 & 0 \end{bmatrix} \mathbf{e} \tag{23}$$

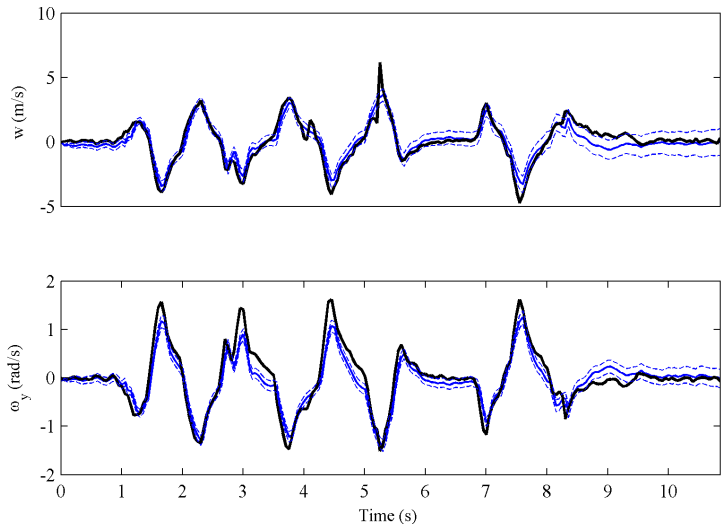

Figure 3. Longitudinal open loop comparison: Measured output (solid black line), Simulated output (solid blue line), Simulated output standard deviation (dashed blue line).

Figure 3 illustrates a comparison between the measured outputs (solid black line) and the simulated outputs (solid blue line) which were obtained with an open loop simulation. The standard deviations of the simulated outputs (dashed blue lines) were calculated with a Monte Carlo simulation involving 300 trials. The perturbation matrix **K** was not used for the simulations. It can be seen that the simulated outputs do not match exactly the measured outputs. However, since the main dynamic characteristics of the system appear to be well captured and the standard deviation is small, it was concluded that the aerodynamic model was suitable for control design.

5. CONTROL

Figure 4 illustrates the longitudinal controller architecture used for hovering maneuvers. The Laplace operator s is dropped for simplicity. In this Figure, only the control of attitude variables ω_y and θ is shown. The displacement speed w is not controlled because it was not a parameter measured by the autopilot. It is worth noting that the Euler angle θ is obtained by conversion of the quaternion error.

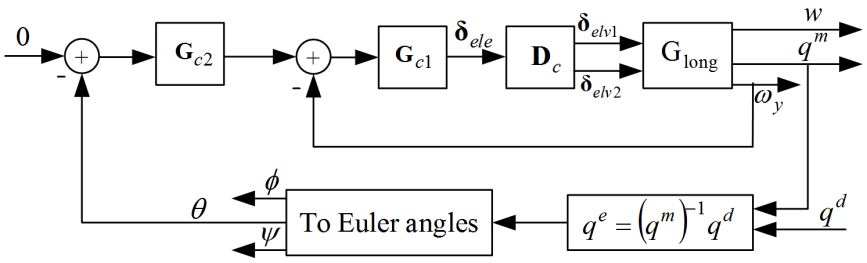

Figure 4. Longitudinal control architecture for hovering mode

The system possesses two elevons which can act like ailerons as well as an elevator. For the longitudinal controller, an elevator command is generated by the inner controller G_{c1} and is transformed into two elevon servo commands with

$$\mathbf{D}_c = \begin{bmatrix} 1 \\ -1 \end{bmatrix} \tag{24}$$

To convert the elevon commands from pulse-width units to degrees of deflection, a gain of 78.0 $\deg/ms$ was used.

Two longitudinal cascaded controller configurations (Table 1) consisting of proportional (P) and proportional-integral (PI) regulators were tested. Configuration 1 was previously studied by [4] for a classic fixed-wing MAV. Configuration 2 moves the PI to the inner loop to provide an anti-windup regulator where the limits are fixed to the deflection limits of the elevons. Tuning was carried out with the contour method based on the Nichols chart and used previously in [3, 4] for a fixed-wing MAV.

Table 1. Controller configurations

Configuration	**External controller** G_{c2}	**Internal controller** G_{c1}
Config. 1	$\dfrac{-6.0(2.0s+1)}{2.0s}$	0.3
Config. 2	–6.0	$\dfrac{0.3(2.0s+1)}{2.0s}$

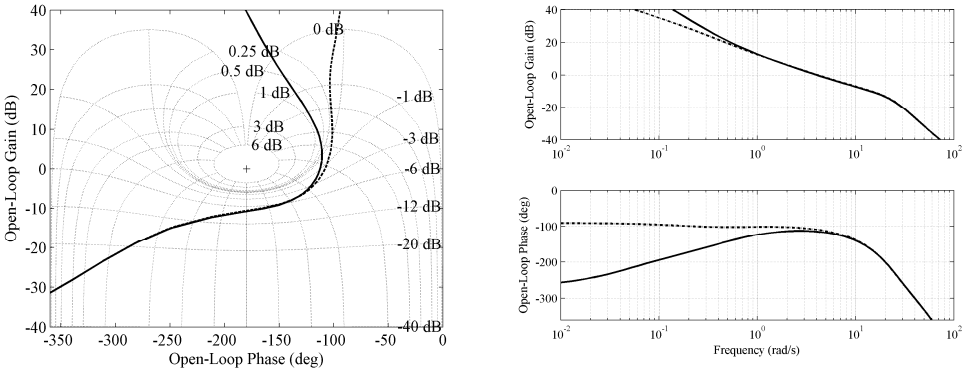

Figure 5. Frequency responses of the external loop: Config. 1 (–), Config. 2 (- -)

By analyzing the frequency responses of the external loops, which are illustrated in Figure 5, it was found that Configuration 2 possessed two advantages over Configuration 1. First, Configuration 2 is subject to less overshoot, and second, the unstable pole of the inner loop is replaced by a stable pole. Examination of the low frequency response showed that Configuration 1 started at -270° while Configuration 2 started at -90°. Table 2 presents a comparison of the properties of both system configurations. From the Table, it can be seen that both configurations possess very similar performance properties. The major difference is the reduction of the resonance factor, M_r, from 1 dB in Configuration 1 to 0.25 dB in Configuration 2. Also, it can be seen that Configuration 2 will allow a non-zero static error for the orientation loop. However, in practice, the accumulation of static error will be unnoticeable because the operator will be constantly commanding the TS-MAV to move from one position to another.

Table 2. Comparison of the properties of the system

Configuration	ω_{co} (rad/s)	ω_{180} (rad/s)	A_m (dB)	ϕ_m (deg)	M_r (dB)
Config. 1	4.01	16.8	11.6	65.4	***1.00***
Config. 2	4.12	16.8	11.4	70.5	***0.25***

ω_{co} : cut-off frequency, ω_{180} : instability frequency, A_m : amplitude margin (open loop), ϕ_m : phase margin (open loop), M_r : Maximum peak resonance factor (closed loop).

Flight tests were carried out with the two controller configurations shown in Table 1 to assess the physical system behavior and to verify the validity of the theory for this application. The rise times for both configurations were very similar and satisfactory for this application. Figures 6 and 7 illustrate that the model parameters identified in Sec. 4 for the control design were reasonable.

The test data clearly demonstrate the overshoot reduction with Configuration 2 when compared to Configuration 1 after the set point changes. The overshoot decreased from nine percent to zero percent in the best cases demonstrating the improved system response with the Configuration 2 control architecture.

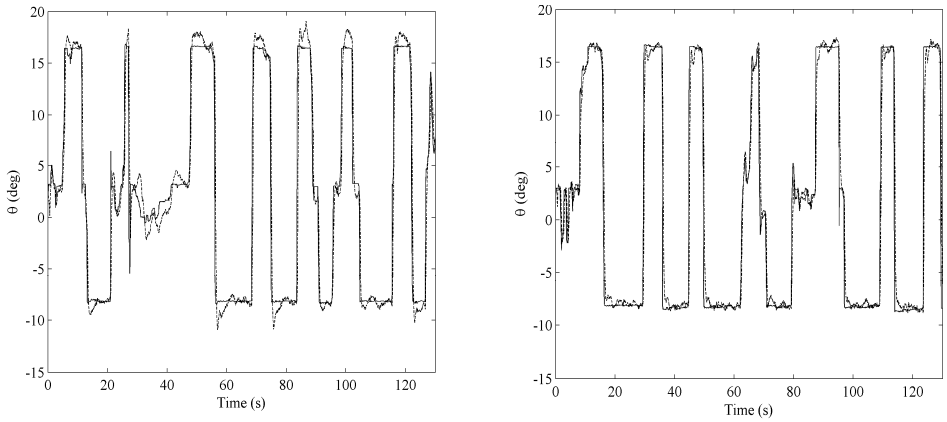

(a) Configuration 1 (b) Configuration 2

Figure 6. Flight test results: Command (−), Response (- -)

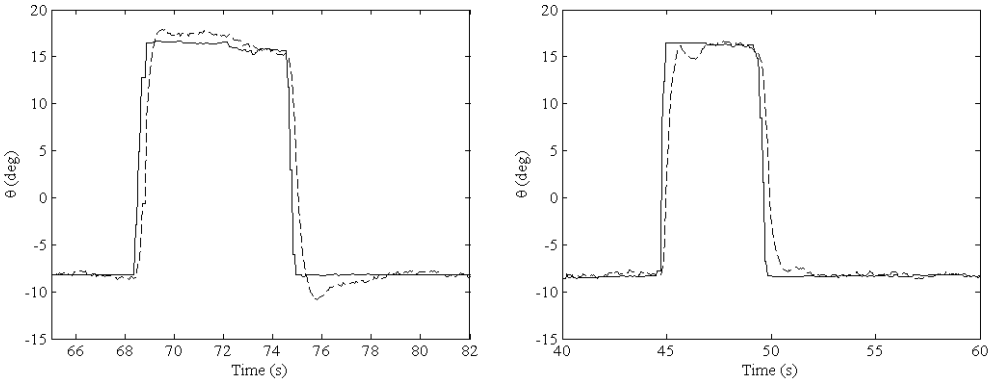

(a) Configuration 1 (b) Configuration 2

Figure 7. Flight test results magnified: Command (−), Response (- -)

6. CONCLUSION

A linear longitudinal model for a hovering tail-sitter MAV was developed. Identification of unknown model parameters was carried out with a multi-variable predictive error method. Two control architectures comprised of proportional and proportional-integral regulators were examined. Controller tuning was accomplished using a frequency method and the Nichols chart. Flight test results showed that a longitudinal cascaded controller with a proportional-integral (PI) regulator in the inner loop was subject to less overshoot when compared to a controller where the regulator was placed in the outer loop. The overshoots were reduced from nine to zero percent in the best cases without penalty to the outer loop global performance thus demonstrating the advantages of placing a PI regulator in the inner loop of the control structure.

Future work with the tail-sitter testbed will involve experimentation and analysis of its response under more aggressive maneuvering commands. The model dynamic equations currently assume that any external disturbances and commands can be treated as small perturbations around a null set point. The flight envelope due to the small perturbation assumption will be explored with the

aim of synthesizing an improved control architecture that will allow the tail-sitter MAV to respond quickly and stably to larger amplitude control inputs.

ACKNOWLEDGEMENTS

The financial support of the Defence R&D Canada Applied Research Project "Extreme Agility Micro-Aerial Vehicle (EA-MAV) Concepts for Complex Terrain Warfare" is acknowledged.

REFERENCES

[1] Directorate of Land Strategic Concepts, *The Army of Tomorrow: Assessing Concepts and Capabilities for Land Operations Evolution*, http://www.army.forces.gc.ca/DLCDDCSFT/pubs/research/The%20Army%20of%20 Tomorrow%20Primer%20Final.pdf, May 2006, 3 Dec. 2009.

[2] Dept. of National Defense, *Integrated Soldier System Project*, http://www.forces.gc.ca/admmat-smamat /projectsprojets2-eng.asp, 2009, 3 Dec. 2009.

[3] Bilodeau, P.-R., *Commande d'un mini véhicule aérien sans pilote en vol stationnaire pour l'opération en milieu restreint*, Master's thesis, Université Laval, 2009.

[4] Bilodeau, P.-R., Poulin, É., Gagnon, E., Wong, F., and Desbiens, A., *Control of a Hovering Mini Fixed Wing Aerial Vehicle*, AIAA Guidance Navigation and Control Conference, Chicago, IL, 2009, AIAA 2009-5794.

[5] Myrand-Lapierre V., A. Desbiens, E. Gagnon, F. Wong and E. Poulin, '*Transitions Between Level Flight and Hovering for a Fixed-Wing Mini Aerial Vehicle*', American Control Conference, Baltimore, Maryland, June 30 - July 2, 2010, Paper WeA15.3.

[6] Myrand-Lapierre, V., *Transition entre le vol non stationnaire et stationnaire d'un véhicule aérien miniature à ailes fixes*, Master's thesis, Université Laval, 2009.

[7] Convair XFY, http://en.wikipedia.org/wiki/Convair_XFY, 2009, Web. 5 Jan. 2010.

[8] Stone, R., *Control Architecture for a Tail-Sitter Unmanned Air Vehicle*, 5th Asian Control Conference, Vol. 2, 2004, pp 736-744.

[9] Knoebel, N. B. and Mc Lain, T., *Adaptative Quaternion Control of a Miniature Tailsitter UAV*, American Control Conference, Seattle, WA, 2008, Paper ThA16.4.

[10] Knoebel, N., *Adaptative Quaternion Control of a Miniature Tailsitter UAV*, Master's thesis, Brigham Young University, 2007.

[11] Osborne, S., *Transitions Between Hover and Level Flight for a Tailsitter UAV*, Master's thesis, Brigham Young University, 2007.

[12] Kuipers, J., *Quaternions and Rotation Sequences*, Princeton University Press, 1999.

[13] Green, W., *A Multimodal Micro Air Vehicle for Autonomous Flight in Near-Earth Environments*, Ph.D. thesis, Drexel University, 2007.

[14] Frank, A., McGrew, J., Valenti, M., Levine, D., and How, J., *Hover, Transition, and Level Flight Control design for a Single-propeller Indoor Airplane*, AIAA Guidance Navigation and Control Conference, Hilton Head, SC, 2007, AIAA 2007-6318.

[15] DeBlauwe, H., Bayraktar, S., Feron, E., and Lokumcu, F., *Flight Modeling and Experimental Autonomous Hover control of a Fixed Wing Mini-UAV at High Angle of Attack*, AIAA Guidance Navigation and Control Conference, Hilton Head, SC, 2007, AIAA 2007-6818.

[16] Stevens, B. and Lewis, F., *Aircraft Control and simulation*, Wiley, 2003.

[17] Gille, J.-C., *Système Linéaires : Équations d'état*, Deuxième Édition, Eyrolles, 1990.

[18] Bilodeau, P.-R., Poulin, E., Wong, F., and Gagnon, E., *Attitude Estimation and Control of a Hovering Mini Aerial Vehicle*, AIAA Guidance Navigation and Control Conference, Toronto, ON, 2010, accepted for publication.

[19] Ljung, L., *System Identification - Theory for the User*, 2nd ed., Prentice Hall, Englewood Cliffs, 1999.